JOURNAL OF AIRCRAFT
Vol. 44, No. 2, March–April 2007

Universality Considerations for Graphing Parachute Opening Shock Factor Versus Mass Ratio

J. Potvin*
Parks College of St. Louis University, St. Louis, Missouri 63103

DOI: 10.2514/1.24061

The parachute opening shock factor C_k is a nondimensional ratio corresponding to the maximum drag F_{max} generated during inflation and is written in terms of the dynamic pressure at the beginning of inflation as well as in terms of the drag area during steady descent. This ratio has been a useful tool for estimating the value of the F_{max} of "off-the-shelf" parachutes used in untested drop conditions or with new canopy dimensions. This paper addresses the issue of the "universality" of plotting C_k vs the mass ratio R_m, which estimates the air mass that codecelerates with the system; that is, whether Ck can be plotted on the same graph, using data collected from parachutes of different canopy shape and porosity, reefing design, etc. The use of the momentum-impulse theorem shows how such a practice is warranted; it shows also how to use the C_k–R_m data of existing parachute systems to get predictions for altogether new and never-tested designs. This approach should be useful also for estimating F_{max} of flown but uninstrumented prototypes, because it allows a calculation based solely on canopy shape and dimensions, reefing design, drop conditions, and on a video study of the inflation time.

Nomenclature

A	=	ballistic parameter
C_D	=	drag coefficient
C_k	=	opening shock factor
C_D^{sd}	=	drag coefficient during steady descent
D_0	=	nominal diameter of parachutes, based on total canopy surface area [1]
dt	=	integration time increment
$F_D(t)$	=	drag force
F_{max}	=	maximum drag sustained during inflation
F_r	=	Froude number
g	=	constant of gravity
I_F^{if}	=	normalized drag integral
m	=	total mass of parachute and payload
n_{fill}	=	standard filling time (see [1])
n_{fill}^{gen}	=	generalized filling time
R_m	=	inverse mass ratio
S_0	=	total canopy surface area (hemispherical canopies) [1]
$(SC_D)_{sd}$	=	drag area during steady descent
$(SC_D)(t)$	=	instant parachute drag area
t	=	time
t_f	=	time at the end of inflation
t_i	=	time at the beginning of inflation
U_{ck}	=	constant defined in Eq. (16)
V_f	=	parachute–payload speed at the end of inflation
V_i	=	parachute–payload speed at the beginning of inflation
V_{ls}	=	parachute–payload speed at the moment of suspension line stretch
V_{sd}	=	parachute–payload speed during steady descent
$V(t)$	=	parachute–payload speed
W	=	parachute–payload weight
Γ	=	momentum–gravitational impulse integral; defined in Eq. (8)
ρ	=	air density at deployment altitude

Introduction

THE opening shock factor C_k is a nondimensional ratio corresponding to the maximum drag force F_{max} generated by an inflating parachute (Fig. 1). This ratio is expressed in terms of the dynamic pressure sustained by the parachute–payload system at the beginning of the inflation process, most typically at the moment of the full stretching of the suspension lines, and also in terms of the parachute's drag area $(SC_D)_{sd}$, generated when the parachute is fully opened and descending in a steady manner [1–3][†]:

$$C_k \equiv \frac{F_{max}}{(SC_D)_{sd}(\frac{1}{2}\rho V_{ls}^2)} \tag{1}$$

Knacke [1], Ewing et al. [2], and then Wolf [3] have shown that graphing C_k in terms of the inverse mass ratio[‡] $R_m \equiv \rho(SC_D)_{sd}^{3/2}/m$ arranges the data of a great many drops into the distinct trend shown in Fig. 2. The value of $(SC_D)_{sd}$ is calculated from the standard steady descent formula, that is, $(SC_D)_{sd} = 2W/\rho V_{sd}^2$. The mass ratio is an estimate of the air mass that decelerates (or accelerates) along with the parachute system during inflation [3]. As such, R_m reveals how important drag is relative to total weight, and hints at which types of deceleration or acceleration profiles (and parachute wakes) are to be anticipated during inflation; for example, parachute systems characterized by $R_m \to \infty$ will tend to decelerate substantially during inflation (when dropped from aircraft), whereas those featuring $R_m \to 0$ will typically move at constant speed along horizontal trajectories or accelerate at a rate mostly controlled by the value of g along nonhorizontal trajectories. Graphing C_k data vs (inverse) mass ratio appears to apply not only to low-porosity hemispherical parachutes used for personnel and cargo drops (including shallow conical parachutes), but also to high-porosity hemispherical canopies such as those used as braking chutes on glider aircraft [1,2,4,5,7–22]. Additionally, the curve appears to handle the data of both parachute types in either unreefed or (permanently) reefed conditions. What makes the opening shock factor so useful in parachute design is that the parameters ρ, R_m, V_{ls}, and $(SC_D)_{sd}$ are either well known or straightforward to estimate,

Received 20 March 2006; revision received 6 June 2006; accepted for publication 6 June 2006. Copyright © 2006 by the American Institute of Aeronautics and Astronautics, Inc. All rights reserved. Copies of this paper may be made for personal or internal use, on condition that the copier pay the $10.00 per-copy fee to the Copyright Clearance Center, Inc., 222 Rosewood Drive, Danvers, MA 01923; include the code 0021-8669/07 $10.00 in correspondence with the CCC.

*Professor, Parks College Parachute Research Group, Department of Physics. Senior member AIAA.

[†]The factor C_k is labeled as C_X in [2]; in [1], it is referred to as C_X only in connection with data collected in wind-tunnel experiments.

[‡]The term *inverse* is used here to distinguish from the ratio $M_r \equiv R_m^{-1}$, which is also called *mass ratio* by other authors 4–6. Such a version of the ratio is not used in this paper.

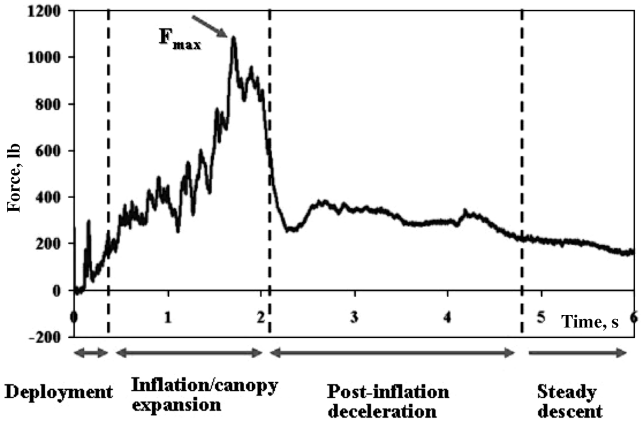

Fig. 1 Sample drag force evolution experienced by a Performance Designs Sabre 150 parafoil (slider-reefed). The detailed description of the canopy dimensions, payload weight and drop conditions can be found in [24].

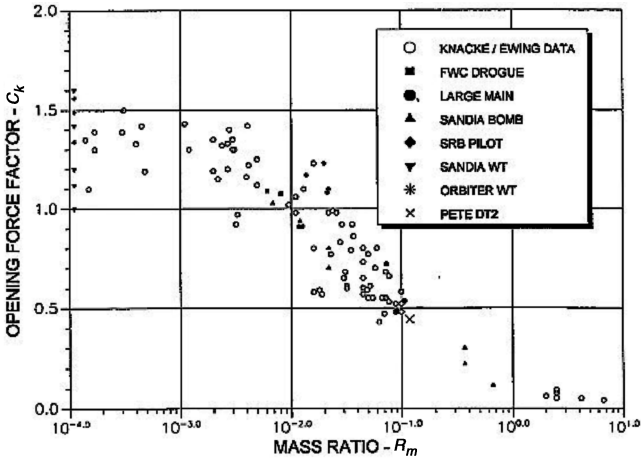

Fig. 2 Wolf's [3] compilation of the opening shock factor vs the inverse mass ratio, for several low- and high-porosity hemispherical parachutes (unreefed and permanently reefed).

thus making possible an extrapolation of C_k from Fig. 2 and the ensuing calculation of $F_{\max}$ from Eq. (1). In other words, the use of the opening shock factor provides the means to make predictions of $F_{\max}$, not only for already-tested parachute systems used in drop conditions involving untested values of payload masses, line-stretch dynamic pressures, or deployment altitudes, but also used at various sizes of the same canopy design. If the C_k–R_m graph were to be truly universal, that is, usable for any parachute and reefing types (including parafoils), the current parachute data contained in Fig. 2 could thus be available to predict opening shock for altogether new designs.

Unfortunately, the universal character of Fig. 2 is cast in doubt when plotting the opening shock factor of hemispherical parachutes reefed at the skirt undergoing disreefing during inflation. Disreefing is a process taking place when the skirt-reefing line is severed by a cutter preset for activation at a given altitude or time [1,2]. The C_k-R_m curve corresponding to such an inflation event is shown here in Fig. 3, a figure that was also created by Wolf [3]. Obviously, the C_k data corresponding to disreefing do not coincide with the no-reefing or permanent-reefing data of Fig. 2.

More problems with the universal character of Fig. 2 appear when attempting to plot the C_k values obtained from unreefed and subscale low-porosity hemispherical parachutes, such as the half-scale cruciform and half-scale USAF C-9 parachutes studied by Potvin et al. [7,23] (the C-9 is a low-porosity hemispherical canopy [1]). In this case, the C_k values at $R_m \sim 1$ were found to be nearly twice the values found in Fig. 2 (i.e., the very figure to which this data ought to

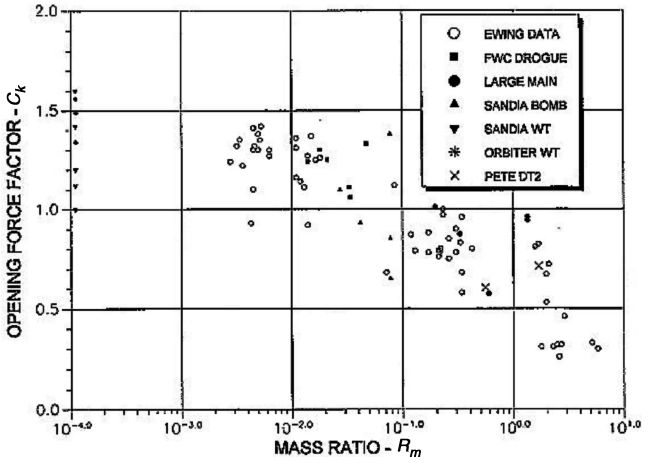

Fig. 3 Wolf's [3] compilation of the opening shock factor vs the inverse mass ratio, for disreefing low- and high-porosity hemispherical parachutes.

belong, because these hemispherical parachutes were unreefed). In fact, such data fit better in the graph of Fig. 3, which so far has been used only for disreefing parachutes. A similar problem is found when dealing with the data of the 3.5%-scale C-9 models (unreefed) that were studied in water-tunnel experiments by Johari and Desabrais [14]; interestingly, such data fit neither of the trends shown in Figs. 2 or 3, because the opening shock factor was found at $C_k \sim 4.7$.

Given the great potential of Fig. 2 for parachute design, it is worth spending time to better understand these discrepancies along with the issue of universality, so to be able to incorporate in that same figure the data from all parachute categories, including clusters [1,2,9,22], crosses [7], parafoils [6,24], deep cones [10], ballutes [1], disk-gap-bands [13,15,19], ribbons [15,16], drive-slotted hemisphericals [20], and all parachute types outfitted with dynamic reefing, such as sliders [11,24]. The truly exciting result of this paper is that all these questions can be answered with the use of one general principle, namely, the momentum-impulse (MI) theorem.

Momentum-Impulse Theorem and Parachute Inflation

As the integral version of Newton's second law of motion, the MI theorem relates the momentum change of a parachute–payload system to the time integral of the net external forces acting on it. Focusing on the axial momentum and force components along the fall trajectory following a drop from aircraft (Fig. 4), one has:

$$mV_f - mV_i = \int_i^f F_D(t)\,\mathrm{d}t + \int_i^f W\cos\theta(t)\,\mathrm{d}t \qquad (2)$$

Here, the flight angle $\theta(t)$ is defined so that a 0-deg value corresponds to a parachute–payload system falling straight down, and a 90-deg value to the system traveling horizontally (and to the right in Fig. 4). Equation (2) is rewritten in terms of Eq. (1) as follows:

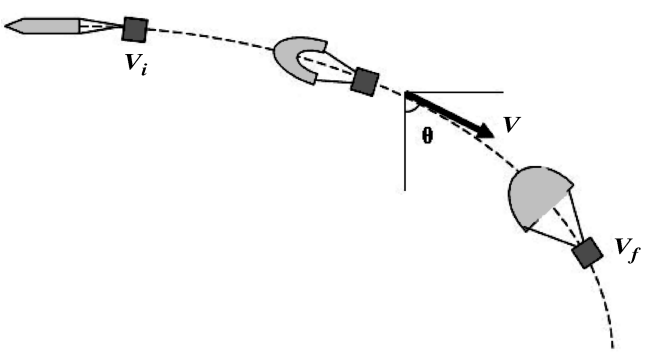

Fig. 4 Definition of the trajectory angle, initial speed, and final speed along the trajectory.

$$(mV_f - mV_i) = -\left(\frac{1}{2}\rho C_k (SC_D)_{\text{sd}} V_i^2 (t_f - t_i)\right) I_F^{\text{if}} + \int_i^f W \cos\theta(t)\,\mathrm{d}t \tag{3}$$

with the normalized drag integral, I_F^{if} defined as

$$I_F^{\text{if}} = \int_i^f \frac{|F_D(t)|\,\mathrm{d}t}{F_{\max}(t_f - t_i)} \tag{4}$$

By definition, $V(t_i) \equiv V_i$ and $V(t_f) \equiv V_f$ refer to the parachute–payload tangential speeds at the beginning and end of the inflation process, respectively. V_i and V_f are always positive, whereas $F_D(t) < 0$ and $F_{\max} > 0$. In practical terms, t_i refers to the moment of suspension line stretch or first "gulp"; and t_f marks, for parachute systems undergoing much deceleration during inflation (i.e., at large R_m), the moment when the canopy has inflated to its steady descent diameter for the first time, as with the openings that yielded the force evolutions shown in Figs. 5–12.[§] In the case of systems that are accelerating or moving at constant speeds (i.e., low R_m, see Fig. 13), t_f typically marks the time of maximum drag force: a time that usually follows the first time extension to steady-state diameter [14]. The inflation time $t_f - t_i$, thus defined, allows its determination from video of the opening process.

In the case of systems that are accelerating or moving at constant speeds (i.e., low R_m), t_f typically marks the time of maximum canopy extension, a time that usually follows first-time extension to steady-state diameter [14]. The interval $t_f - t_i$ thus defined allows its determination from video of the opening process. On the other hand, the drag integral I_F^{if} contains the information related to the normalized shape of the F_D vs t curve, and is a measurement of the area under that curve. This feature makes the details of the drag evolution somewhat less important to the overall momentum change of the system; moreover, I_F^{if} is more or less independent of the actual value of $F_{\max}$. Equation (3) can now be solved for C_k, yielding

$$C_k = \left(\frac{m}{(1/2)\rho(SC_D)_{\text{sd}}^{3/2}}\right) \times \left(\frac{(SC_D)_{\text{sd}}^{1/2}}{V_i(t_f - t_i)I_F^{\text{if}}}\right) \frac{-(V_f - V_i) + \int_i^f g\cos\theta(t)\,\mathrm{d}t}{V_i} \tag{5}$$

Equation (5) is rewritten as follows:

$$C_k = \frac{2}{R_m n_{\text{fill}}^{\text{gen}}}\Gamma \tag{6}$$

This result involves two integral-based inputs, namely, the generalized nondimensional filling time

$$n_{\text{fill}}^{\text{gen}} \equiv \frac{V_i(t_f - t_i)}{(SC_D)_{\text{sd}}^{1/2}} I_F^{\text{if}} \tag{7}$$

and the momentum–gravitational impulse (MGI) integral

$$\Gamma \equiv \frac{-(V_f - V_i) + \int_i^f g\cos\theta(t)\,\mathrm{d}t}{V_i} \tag{8}$$

The first term in the MGI integral corresponds to the parachute–payload system's net change of momentum (per unit mass and per unit speed). The second term represents the momentum gained by the system and, subsequently, partly lost through drag, while in the process of being pulled by gravity. Note that external forces other than gravity, such as rocket thrust on an ejection seat, would appear in this second term as well, when relevant to the problem at hand. In such cases, however, the connection herein assumed between R_m and the deceleration/acceleration profile of the system no longer holds. This issue shall be discussed further in a future publication.

Given the generality of the MI theorem, plotting C_k data in terms of the inverse mass ratio, generalized filling time, and MGI integral lead to a curve that is truly (and trivially) universal. The generalized filling time is somewhat different from the more familiar filling time $n_{\text{fill}} \equiv (t_f - t_i)V_i/D_0$ used in parachute engineering [12,14]. Here, D_0 is the so-called nominal canopy diameter, calculated from the total canopy surface area S_0 as $D_0 = (4S_0/\pi)^{1/2}$. [1] (For parafoils, S_0 is given by the product of the chord and span [6].) Obviously, $n_{\text{fill}}^{\text{gen}}$ contains additional information related to the explicit evolution of the drag force (i.e., through I_F^{if}). But both are related, as will be discussed further in the next section. On the other hand, the MGI integral assumes much-simplified forms for inflation sequences taking place either along the horizontal or vertical, namely, $\Gamma = 1 - V_f/V_i$ and $\Gamma = 1 - V_f/V_i + (g/V_i)(t_f - t_i)$, respectively.

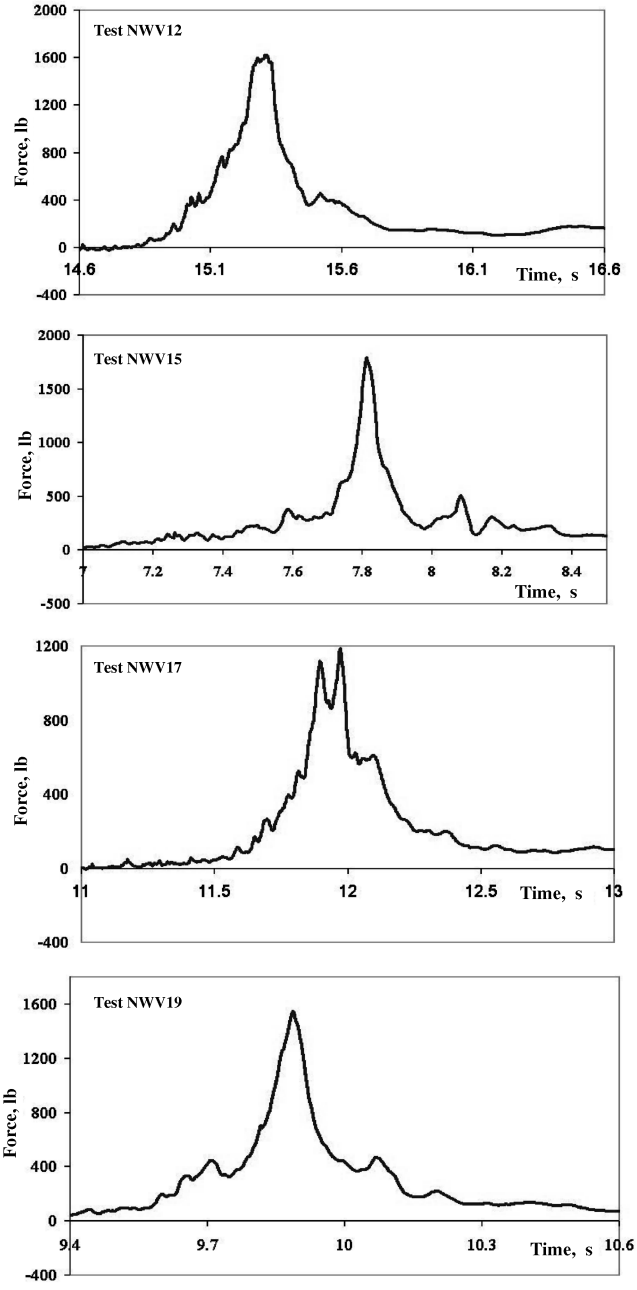

Fig. 5 Drag evolutions of a half-scale USAF C-9 parachute (a low-porosity, unreefed hemispherical parachute) [7]. From top to bottom, the drag integral corresponding to each test is as follows: $I_F^{\text{if}} = 0.39$, 0.35, 0.43, and 0.40. The parachute carried a 105-lb payload.

[§]Other authors have resorted to a somewhat different definition, instead using the value of $(SC_D)_{\text{sd}}$, being reached for the first time as a marker for t_f (see, for example, [1], Sec. 5.4.4; see also [12]). This alternate criteria involves knowing the temporal evolution of $SC_D(t)$, an input that is rarely available in the usual testing environment.

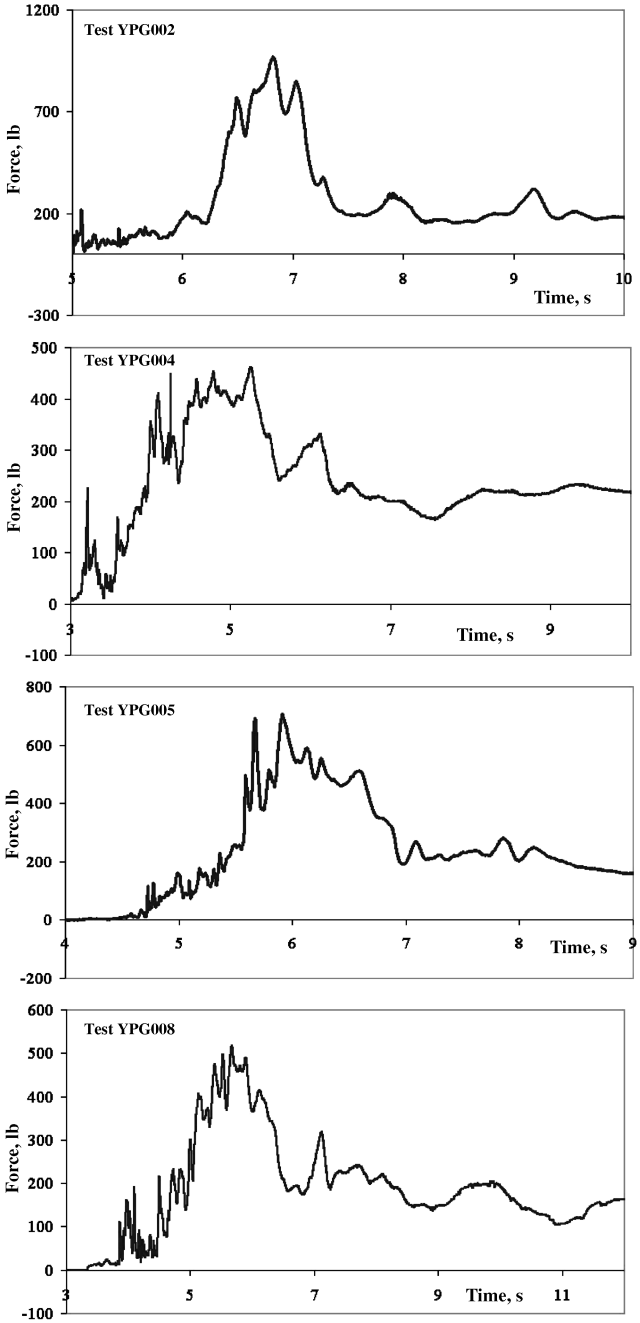

Fig. 6 Drag evolutions of a full-scale USAF C-9 parachute (a low-porosity, unreefed hemispherical parachute) [18]. From top to bottom, the drag integral corresponding to each test is as follows: $I_F^{\text{if}} = 0.54, 0.71, 0.59$ and 0.66. A payload weight of 165 lb was used in all drops.

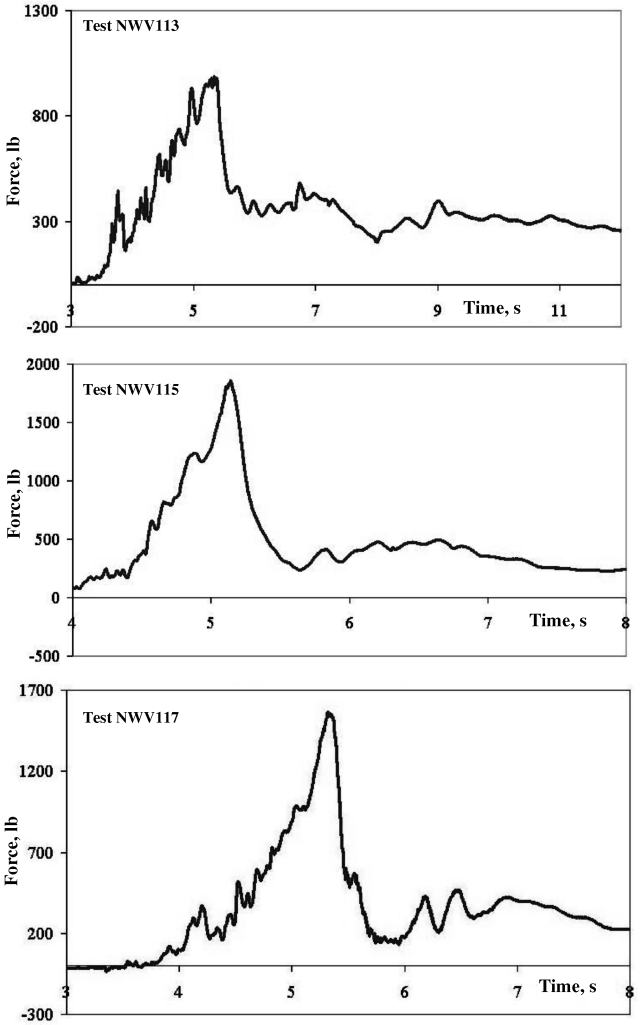

Fig. 7 Drag evolutions of a U.S. Navy emergency personnel parachute (a low-porosity, unreefed conical parachute for a NB-8 pack) [7]. From top to bottom, the drag integral corresponding to each test is as follows: $I_F^{\text{if}} = 0.58$, 0.56 and 0.43. The payload weight was set at 290 lb in all drops.

These examples show clearly how Γ depends on deployment conditions and payload weight (through V_i), as well as on the actual inflation evolution [through V_f and $(t_f - t_i)$].

Finally, remember that the derivation has (implicitly) involved only one assumption, namely, that of considering the drag force being tangential to the flight trajectory. In principle, the use of such an assumption excludes the C_k data of any gliding parachute types, either hemisphericals with drive slots or parafoils. But this exclusion has minimal consequences in practice, because most gliding parachutes used nowadays have either been rigged for zero glide or exhibit very poor gliding characteristics during inflation.

As a historical note, it has to be mentioned that over a decade ago, Niemi, Jr. [25] used the impulse connected to the drag force (in nondimensional form) to plot, as a function of the Froude number ($F_r \equiv V_{\text{ls}}^2/gD_0$), the drag data of USAF C-9 canopies as well as of subscale and full-scale C-9 models made of different fabric [4,21]. Niemi obtained an excellent correlation that collapsed lots of seemingly unrelated parachute data onto a single curve. However, by neglecting the gravitational contribution to the impulse, the correlation is missing a filling-time-dependent term that is responsible for most of the residual scatter showing in the collapsed data. The use of Eq. (6) will show how to correctly include the gravitational impulse in Froude number scaling, and in a manner applicable to all canopy and reefing types.

C_k Versus R_m: A New Perspective

Dependence on Filling Time

The presence of the nondimensional filling-time factor in the denominator of Eq. (6) underlines the importance of inflation duration in determining C_k. It also explains why C_k values for disreefing parachutes (Fig. 3) did not coincide with the data of Fig. 2, because disreefing chutes exhibit shorter nondimensional filling times compared with those of unreefed or permanently reefed parachutes. Typically, theirs is in the $n_{\text{fill}} = 2$–7 range, vs $n_{\text{fill}} =$ 6–14 for unreefed or permanently reefed parachutes [1], depending on reefing ratio, canopy porosity, etc. To put it in another way, the data of Fig. 3 are not so much different from those of Fig. 2 because of disreefing per se, but rather because of the smaller values of the filling time that are associated with disreefing. This means that other canopy and reefing types, with or without disreefing, should also fit well the trend of Fig. 3 if likewise characterized by small n_{fill} values. Such is

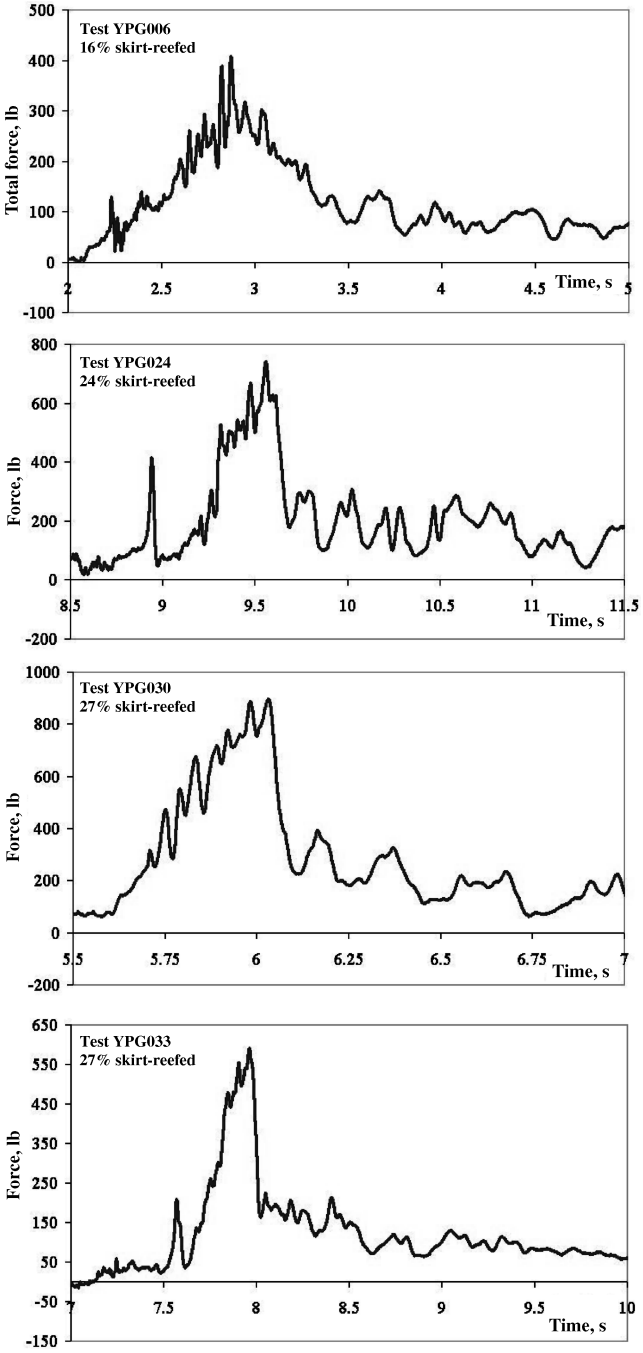

Fig. 8 Drag evolutions of a skirt-reefed, half-scale USAF C-9 parachute [18]. From top to bottom, the drag integral corresponding to each test is as follows: $I_F^{\text{if}} = 0.51, 0.50, 0.57$ and 0.60. The payload weight was set at 66 lb in all drops.

indeed the case, for example, with unreefed parafoils [6] and with the subscale hemispherical parachutes of [7,23] (also unreefed), two examples for which $n_{\text{fill}} \sim 2$. (The unusually small n_{fill} value for the canopies of [7,23] came from the initial canopy mouth being forced open to a larger diameter because of the larger-than normal riser-to-riser separation and larger payload container width.)

It has to be pointed out that the importance of n_{fill} explains, but only partially, why the 3.5%-scale C-9 data of [14] do not fit either Figs. 2 or 3. Like with other subscale cases, these data again feature $n_{\text{fill}} \sim 2.5$; but being associated with a water-tunnel experiment, it has also a lower value of the drag integral I_F^{if}, an effect that will be explained further in the next section. This, in turn, yields a lower generalized filling time $n_{\text{fill}}^{\text{gen}}$, a value that drastically increases C_k when used in Eq. (6).

Mass-Ratio Dependence

The second interesting feature of Eq. (6) is its explicit $1/R_m$, a dependence that is clearly seen in Fig. 2 at large values of the inverse mass ratio (see also [2]). The MGI integral is also quite sensitive on R_m, but only implicitly, and in the following general manner: $\Gamma \to 1$ when $R_m \to \infty$; and $\Gamma \to 0$ as $R_m \to 0$. As discussed later, there is also an R_m dependence associated with the drag integral I_F^{if}, a dependence that is rather mild. Finally, the standard filling time n_{fill} depends on mass ratio as well, but also mildly in most modern parachute applications. The R_m dependence of n_{fill} is understandable given that at very low R_m, inflation will always involve larger (air) fluxes through the canopy mouth, and therefore a shorter n_{fill}, than at very high R_m. This follows from the system traveling at constant or increasing fall speed over time at low R_m and at decreasing fall speed at high R_m. Several investigations and models bear these facts out [5,20,25–29], for example, in the case of the C-9 canopy, one has $n_{\text{fill}} = 5.68 + (0.0501\rho D_0^3/m)$ [5,20]. However, these studies show the effect to be observable only when $\rho D_0^3/m > 10$, that is, at a range that corresponds roughly to $R_m > 10$ and in which very few parachute applications operate. Interestingly, Barnard [27] shows that in the limit $R_m \to 0$, the value of n_{fill} becomes very sensitive to canopy mass rather than payload mass (and mass ratio) when the former becomes similar to, or larger than, ρD_0^3, a limit that becomes significant only at altitudes exceeding 100,000 ft (at least for parachute systems built with today's design specifications and construction).

With these remarks in mind, the R_m dependence of the opening shock factor becomes clear: in the $R_m > 10^{-1}$ regime, the payload mass is comparable in magnitude to that of the air codecelerating with the opening parachute, a condition that causes substantial deceleration of the system during inflation. It follows that for horizontal drops from fast aircraft (typically, 150 KIAS or greater), one has $V_f \ll V_i$,

$$\Gamma_t \sim 1 - V_f/V_i \sim 1$$

and, therefore,

$$C_k \sim 2/(n_{\text{fill}}^{\text{gen}} R_m)$$

At the other end of the mass-ratio range (i.e., $R_m \to 0$), in which codecelerating air mass is much smaller than parachute–payload mass, there is no appreciable deceleration during inflation along horizontal trajectories, a condition that results in $V_f/V_i \sim 1$ and $\Gamma \to 0$. Along vertical trajectories, on the other hand, or any other nonhorizontal trajectories for that matter, the system picks up speed at more or less the rate dictated by gravity, given that $F_D \ll W$, again a case for which $\Gamma \to 0$. So, in the limit for which $R_m \to 0$, one has $(R_m)^{-1} \to \infty$ and $\Gamma \to 0$, that is, limits that lead to an indetermination and to the plateau-convergence seen in the low-R_m side of Fig. 2. Note that this portion of Fig. 2 also includes inflation data from wind-tunnel tests, a type of experiment that should be considered a limit case of the MI theorem, as will be discussed later.

Drop-to-Drop Variations

Equations (6–8) also offer a strategy for estimating the effects of inflation performance variability on a drop-to-drop basis. Drop-to-drop variations of inflation performance have their roots in the fact that all parachutes are in a limp state after being extracted from their bag and exposed to the airstream for the first time (the moment of the first gulp). Such a state leads not only to variations in initial parachute mouth area (or wing inlet area in the case of parafoils), but also in air flux into the canopy, filling-time values, and ultimately drag evolutions. Drop-to-drop variations are obvious in Figs. 5–8 and in Fig. 11. Interestingly, these figures show that such variations affect more the value of the (dimensional) inflation time $t_f - t_i$ than the overall shape of the drag evolution. Note that the value of $n_{\text{fill}}^{\text{gen}}$ will more likely change because of variations in $t_f - t_i$ (and n_{fill}) than variations of I_F^{if} (more on this, next). Note, finally, that the variations of the opening shock factor will also depend on the value of V_i, which is also expected to vary on a drop-to-drop basis. This is due mainly to

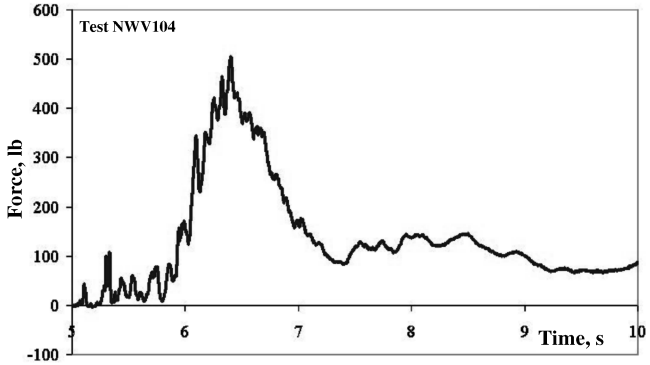

Fig. 9 Sample opening force evolution of a U.S. Army cruciform parachute (unreefed; 24-ft-long panels of 2.6-to-1 aspect ratio) [7]. The drag integral corresponding to this test is $I_F^{\text{if}} = 0.58$. The payload weight was set at 110 lb for this test.

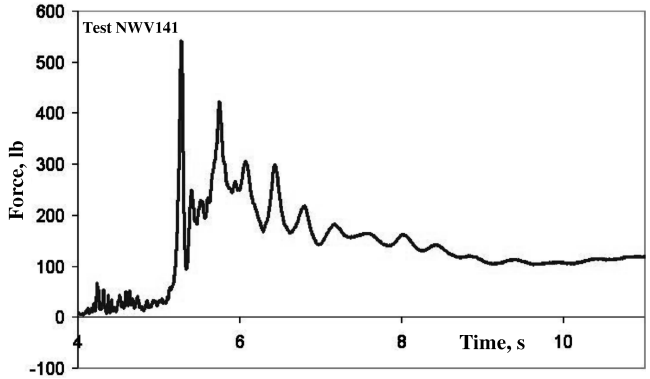

Fig. 10 Drag evolution of a U.S. Army 26-ft ringslot parachute (unreefed) [7]. Note that the tall and narrow peak on the left is not part of the inflation process, but corresponds to the moment at which the canopy has been extracted out of its bag. The drag integral corresponding to this test is $I_F^{\text{if}} = 0.59$. The payload weight was set at 123 lb.

the flying of slightly different drop runs during repeated tests and to varying payload dynamics before parachute inflation. Their variability can be assessed as well, given that these two effects can be studied with computer simulations of preinflation (see [17], for example).

Comparison with Another Derivation of C_k

It should be mentioned that the close connection between C_k and the product $R_m n_{\text{fill}}$ can be obtained from a formalism developed by Pflanz [1,30], Ludtke [31], and Doherr [12], albeit in a more restricted application. This is achieved by integrating Newton's equation of motion while using a time polynomial to describe the evolution of the drag area:

$$2F_D(t)/\rho V(t)^2 = (SC_D)(t) = (SC_D)_{\text{sd}}[t/(t_f - t_i)]^j$$

with exponent j depending on the type of parachute and reefing (for example, $j \sim 6$ for unreefed, low-porosity hemispherical parachutes; more values can be found in [12]). Such a description has been validated with wind-tunnel data [1] as well as with high-R_m cases [7,23]. In general, the resulting $F_D(t)$ will look like a simple peaked function with the right width and height, but missing the usual local high-frequency bumps and shoulders (see, for example, [23]). In cases for which $F_{\max}$ occurs before $t = t_f$, Doherr [12] calculated (horizontal inflation)

$$C_k = \left(\frac{j+2}{2(j+1)}\right)^2 \left(\frac{j(j+1)A}{j+2}\right)^{\frac{j}{j+1}} \tag{9}$$

where the ballistic parameter [1], a nondimensional ratio, is defined as

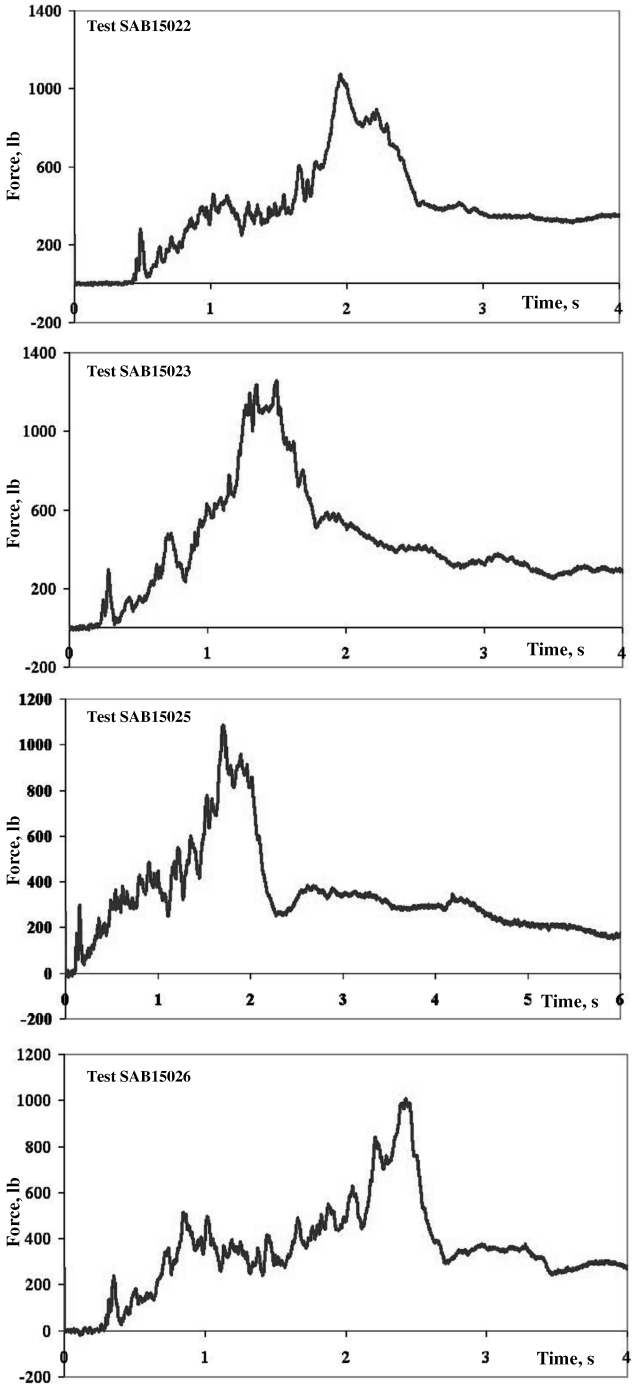

Fig. 11 Drag evolutions experienced by a Performance Designs Sabre 150 parafoil (slider-reefed) [24]. From top to bottom, the drag integral corresponding to each test is as follows: $I_F^{\text{if}} = 0.48, 0.50, 0.47$ and 0.44.

$$A = \frac{\sqrt{\pi C_D^{\text{sd}}}}{R_m \cdot n_{\text{fill}}} \tag{10}$$

(Doherr [12] obtained a similar expression when $F_{\max}$ occurs at or after $t = t_f$.) The similarity with Eq. (6) is uncanny because $j/j + 1 \sim 1$ (for $j > 3$), despite the presence of factors that are clearly related to the specific drag area model being used. Interestingly, both Eqs. (6) and (9) could be used together to narrow down (predict?) the appropriate value of the exponent j in the drag area law.

Doherr's approach [12] shows that expressing C_k in terms of the combination of the nondimensional parameters featured in Eq. (6) is not unique, obviously. But such a choice was made on purpose, to keep explicit the three major elements of the momentum-impulse

theorem, namely: momentum transfer, force applied, and duration of force applied.

Drag Integral Calculation

The usefulness of Eq. (6) in parachute design depends in no small part on being able to approximate or predict the value of the normalized drag integral I_F^{if}. Fortunately, it is possible to do so because, as stated previously, I_F^{if} is less dependent on the detailed evolution of the drag force. This is shown explicitly by the analysis of the experimental parachute drag data shown in Figs. 5–12. These showcase the results of test drops from aircraft flying at 90 to 110 KIAS, and up to an altitude of 5000 ft mean sea level (MSL). The payload weights and parachute sizes used in those tests resulted in medium-to-high mass-ratio drops, that is, $R_m > 10^{-1}$ [7,23,24]. On the other hand, the data of Fig. 13 were collected during a series of wind-tunnel tests of various disk-gap-band parachute designs being investigated for use by the NASA Mars Exploration Rover (MER) program [13,19]. Not shown in the figures, but also used for this discussion of the drag integral, are the water-tunnel data on 12-in. C-9 parachute models presented in [14]. These two sets of data represent another mass-ratio regime that is also important for parachute design, namely, $R_m = 0$. Thus, the parachutes represented in the figures span all the important categories in use today.

The availability of the F_D vs t data in each of the figures made possible the direct calculation of the drag integral using an Excel-type spreadsheet.[‖] The value of t_i was chosen by visually spotting the beginning of the rise of the main peak; the value of t_f was reached by picking the halfway point of the back side of the peak for the large-R_m cases, in an attempt to locate the beginning of the post-inflation deceleration phase (see Fig. 1). Clearly, determining t_f in this manner and without the supporting tagging signals or detailed video is an approximation, but one that should yield a tolerable error in the ~10–20% range in cases consisting of low-porosity canopies, such as those discussed in Figs. 5–11. For the $R_m = 0$ cases, on the other hand, the value of t_f was made to coincide with the location of $F_{\max}$ because, in this mass-ratio regime, the peak force is usually reached at the end of inflation [1,13,14].

Looking at Figs. 5–12 first, the resulting drag integral is found to be in the range of $I_F^{\text{if}} \sim 0.24$–$0.70$, with the largest number of tests resulting in $I_F^{\text{if}} \sim 0.50$. Interestingly, repeat drops of the same parachute–payload system yielded very consistent values, changing only by 10 to 20%. These data also show clearly the insensitivity of I_F^{if} to the specific value of $F_{\max}$ or of the filling time (as expected). Finally, note that small-I_F^{if} cases (i.e., $I_F^{\text{if}} \sim 0.2$, see Fig. 12) tend to reflect a very slow and low-drag initial inflation, followed by a large but very brief force. On the other hand, the wind-tunnel data of Fig. 13 and water-tunnel data of [14] suggest drag integral values of $I_F^{\text{if}} \sim 0.15$–$0.22$, a very narrow range considering the large differences in constructed diameters (i.e., 12 in. vs 44 ft), porosity and Reynolds number (i.e., 10^4 vs 10^7). Again such values appear to be reached as the result of the inflation curves featuring substantial drag peaks only towards the very end of the inflation sequence. Overall these data suggest a weak-to-moderate dependence of the drag integral on the value of the mass ratio, namely $I_F^{\text{if}} \sim 1/2 \pm 50\%$ at high mass ratios and $I_F^{\text{if}} \sim 1/5 \pm 30\%$ at low mass ratios.

The meaning of the drag integral can be probed further by combining the definitions of both generalized [i.e., Eq. (7)] and standard filling times:

$$n_{\text{fill}}^{\text{gen,acft}} = n_{\text{fill}} \frac{D_0}{(SC_D)_{\text{sd}}^{1/2}} I_F^{\text{if}} \tag{11}$$

Note that $D_0/[(SC_D)_{\text{sd}}]^{1/2} = 2/(\pi C_D^{\text{sd}})^{1/2}$ for both hemispherical and parafoil canopy types, with $C_D^{\text{sd}} \sim 1$ for parafoils. The appearance of the drag integral in Eq. (11) makes the point that $n_{\text{fill}}^{\text{gen}} \sim n_{\text{fill}}$ when $I_F^{\text{if}} \sim 1$, that is, when the opening force is pretty much sustained at its maximum level throughout the inflation process. On the other hand,

[‖]Experimental $F_D(t)$ vs t data points were also supplied to this writer by the authors of [13,14].

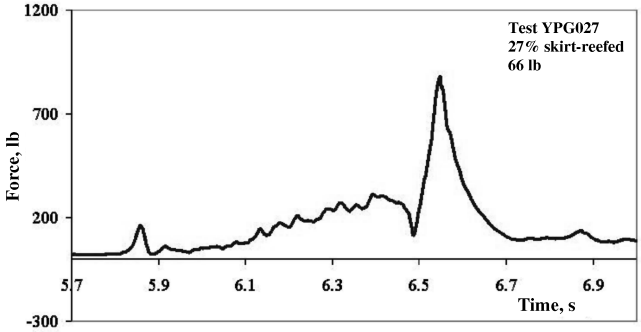

Fig. 12 Drag evolution of a disreefing, low-porosity parachute. Same parachute and payload as the system featured in Fig. 8. Disreefing occurred accidentally when the reefing line broke just before the 6.5 s mark. The drag integral corresponding to this test is $I_F^{\text{if}} = 0.24$.

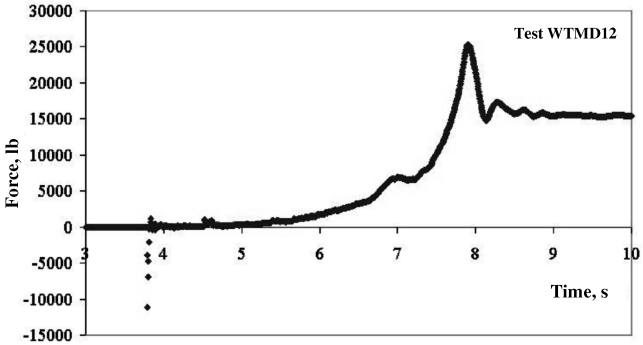

Fig. 13 Sample opening force evolution of a MER disk-gap-band parachute inflating in the NASA Ames full-scale wind tunnel [13,19]. The parachute was deployed at the 3.8 s mark and inflation begun at the 4.6 s mark. The drag integral corresponding to this test is $I_F^{\text{if}} = 0.23$, a very typical value for all of the disk-gap-band parachutes tested for the MER program.

$n_{\text{fill}}^{\text{gen}} \ll n_{\text{fill}}$ when $I_F^{\text{if}} \ll 1$, that is, when most of the inflation dynamics generates low-level drag during most of the process, to be followed by a high but brief drag peak. In other words, $n_{\text{fill}}^{\text{gen}}$ represents the filling time associated with the dominant peak of the F_D vs t curve.

Universal Families of the C_k–R_m Graph

Equation (6) expands the range of validity of the C_k–R_m approach, as well as its applicability to all parachute types, an expansion that goes well beyond a classification based solely on reefing/disreefing configuration [1–3]. This is particularly important given that little opening force data on the newer parachute designs, such as parafoils, have so far been published in the public domain. This expanded C_k–R_m method will allow designers to use hemispherical parachute data to support force estimates aimed at the newer designs. The price to pay for this kind of extrapolation is, of course, the necessity of knowing n_{fill} a priori, that is, knowing an actual inflation performance characteristic. But this price may not be as high given the large amount of filling-time data that is already in the public domain, including data for the newer designs; see, for example, the references listed earlier. In the absence of such data, best case and worst case scenarios may be considered when using filling-time data of parachute systems that have similar disreefing hardware, porosity, and aerodynamics (i.e., wakes).

It is to be pointed out that the filling time can always be inferred simply from the video footage of test drops and from an estimate of V_{ls}. In this regard, the proposed C_k–R_m approach may prove very useful for the estimation of $F_{\max}$ sustained by uninstrumented parachute prototypes, because the method requires only the basic canopy and reefing design and dimensions [for $(SC_D)_{\text{sd}}$], drop condition parameters (for ρ and V_{ls}), and a video study of the filling

time. This is a significant bonus because the video measurement of the filling time (with time stamp) is a much simpler process than the measurement of $F_{\max}$, which involves the use of load cells and other specialized hardware.

In principle, this expansion of the C_k–R_m method should involve different C_k–R_m graphs, each characterized by differing values of the quotient $\Gamma/n_{\text{fill}}^{\text{gen,acft}}$. But the lack of data on Γ for nonhorizontal and nonvertical trajectories prevents such a strategy. An alternate, and perhaps "universal enough" approach could consist in neglecting the contribution of Γ altogether and graph all parachute data on either Figs. 2 or 3, that is, based on whether $n_{\text{fill}}^{\text{gen}} \sim 4$–14 (Fig. 2) or $n_{\text{fill}}^{\text{gen}} \sim 1$–4 (Fig. 3). Here, the quasiuniversality of the approach is insured by making sure that the actual values of the (generalized) filling time are taken into account. In such a scheme, the plotted data would still show a scatter of the type shown currently in Figs. 2 and 3, a scatter resulting from: 1) an implicit dependence on Γ, 2) an implicit dependence on $n_{\text{fill}}^{\text{gen}}$ (but over a narrow range), and 3) on the usual drop-to-drop variations in $n_{\text{fill}}^{\text{gen}}$. An obviously better approach would involve increasing the number of $n_{\text{fill}}^{\text{gen}}$-based graphs, depending on whether $n_{\text{fill}}^{\text{gen}} \sim 1$ to 2, ~2 to 3, ~3 to 4, and so on. But at present there is not enough experimental data available to meaningfully fill up each one of these graphs.

Note that the lower bound on the redefinition of Fig. 3, that is, $n_{\text{fill}}^{\text{gen}} > 1$ (but smaller than 4), is suggested by the water-tunnel/subscale C-9 data of [14]. This is so because, although featuring $n_{\text{fill}} \sim 2.5$, such data are actually characterized by $n_{\text{fill}}^{\text{gen}} \sim 0.5$ and $C_k \sim 4.6$, that is, data that cannot fit in that figure. This example points out the importance of both the standard filling time n_{fill} and drag integral I_F^{if} in defining the universal contents of C_k vs R_m graphs. But settling on the likely value of $n_{\text{fill}}^{\text{gen}}$ may be the difficult step, especially when applied to never-flown parachutes. The previous discussion on the drag integral suggests that assigning $I_F^{\text{if}} \sim 1/2 \pm 50\%$ uncertainty would be a good start for medium-to-high (inverse) mass ratios and $I_F^{\text{if}} \sim 1/5 \pm 30\%$ at medium-to-low mass ratios.

As a first example for using Figs. 2 or 3 to estimate $F_{\max}$ of prototypes carrying limited instrumentation, consider the half-scale USAF C-9 parachute data discussed in [7,23] (no reefing, see representative drag evolutions in Fig. 5). In this case, $D_0 = 14$ ft, $W = 110$ lb, $\rho = 0.0021$ slugs/ft^3, and $R_m \sim 0.88$. The value of n_{fill} was determined by a video study of t_{fill}, coupled with a computer simulation of the preinflation phase (i.e., payload fall and parachute deployment), a study that resulted in $n_{\text{fill}} \sim 1.5$–3.0 over four repeated drops (the parachute was deployed by a static line attached to the aircraft). Assuming the standard $C_D^{\text{sd}} \sim 0.8$ for low-porosity hemispherical canopies [1] and using Eq. (11) with $I_F^{\text{if}} \sim 1/2$, one gets $n_{\text{fill}}^{\text{gen}} \sim 0.63$ and $n_{\text{fill}} \sim 0.95$–1.90; that is, values that would assign this experimental data to Fig. 3, the so-called low filling-time universal C_k–R_m graph, thus yielding $C_k \sim 0.5$–1.0. The uncertainty quoted here refers to the variation associated with the unknown value of Γ and with the natural drop-to-drop variation of the filling time that is also inherent to the data of Figs. 2 and 3. With regards to the latter, the method thus predicts how $F_{\max}$ is likely to vary on a drop-to-drop basis. Finally, this calculation can be compared with one performed with Eq. (6) evaluated with $\Gamma \sim 1$, that is, for a horizontal trajectory while assuming $V_i \gg V_f$: $C_k \sim 2/(R_m n_{\text{fill}}^{\text{gen}}) \sim (2/R_m)$ (0.52-to-1.05) ~1.13-to-2.27 (at $R_m = 0.88$). But this estimate has a large error, given that in the case at hand $V_i/V_f \sim 0.35$, a condition that violates somewhat the constraint $V_i \gg V_f$ (even though the test parachutes indeed inflated horizontally).

The second example illustrates how to use Eq. (6) to analyze data that are not included in Figs. 2 and 3 due to their very small $n_{\text{fill}}^{\text{gen}}$. Considering again the water-tunnel data of Johari and Desabrais [14] on 3.5%-scale C-9 parachute models [14] and comparing with the full-scale (C-9) flat circular parachute data of Knacke [1] (in wind-tunnel conditions), one has at $R_m = 0$: $C_k = 4.7$ [14] vs $C_k = 1.7$ [1] and $n_{\text{fill}} \sim 2.5$ [14] vs $n_{\text{fill}} \sim 8.0$ [1]. Here, the difference in n_{fill} arises from the subscale models opening like umbrellas (i.e., with their skirt spreading early) rather than like normal parachutes (i.e., with their skirt spreading late). Assuming Γ/R_m and I_F^{if} to be the same in both cases (given the same mass ratio and canopy shape, and no reefing), the calculation of the ratio C_k/C_k ([12] and [1], respectively) via Eq. (6) thus yields $C_k \sim C_k$ ([12] and , respectively) and $n_{\text{fill}}/n_{\text{fill}} \sim 5.4$ ([1] and [12], respectively): a result that is pretty close to the experimental value. Here, the 12% discrepancy has to do with Γ/R_m and I_F^{if} being somewhat different, as discussed further in the next section. This is good progress, anyway, given that this is the first time that the C_k values of this water-tunnel study have been reconciled with the rest of the world's opening shock data.

Direct $F_{\max}$ Calculations: A New Window on Inflation

Going well beyond the use of the momentum-impulse theorem as an organizing principle to plot parachute data, it is useful at this point to introduce several of the simplified results that emerge directly from Eqs. (1) and (6), in either the large- or small-R_m limits. Although approximations, these new results apply to any parachute systems and provide simple derivations of several long known parachute inflation facts, which so far have been demonstrated only empirically.

High Mass-Ratio Regime

Considering inflation processes taking place along horizontal or vertical trajectories and focusing on cases where $V_f \ll V_i$, one has access to a set of formulas for the maximum drag force itself, obtained by combining Eqs. (1), (6), and (8):

Horizontal inflation

$$F_{\max} = (SC_D)_{\text{sd}} \left(\frac{1}{2}\rho V_{\text{ls}}^2\right)\left[\frac{2}{R_m n_{\text{fill}}^{\text{gen}}}\right] \qquad V_i \gg V_f \tag{12}$$

Vertical inflation

$$F_{\max} \equiv (SC_D)_{\text{sd}} \left(\frac{1}{2}\rho V_{\text{ls}}^2\right)\left[\frac{2}{R_m n_{\text{fill}}^{\text{gen}}}\left(1 + \frac{gD_0}{V_{\text{ls}}^2} n_{\text{fill}}\right)\right] \qquad V_i \gg V_f \tag{13}$$

Note that the condition $V_f \ll V_i$ limits the range of relevant mass ratios to about $R_m > 10^{-1}$. This is not so bad given that this range applies to many personnel and cargo parachutes dropped from fast-flying aircraft. Left out are low (inverse) mass ratio parachute systems such as drogues and other highly loaded parachute applications [1,13,19], systems that shall be discussed later. Note also that V_i was set to V_{ls}, the system's fall rate at line stretch, and that the gravity-impulse term $(g/V_i)(t_f - t_i)$ in Eq. (13) was rewritten according to Eqs. (7) and (11).

Equations (12) and (13) emphasize the dependence of maximum drag on the mass ratio R_m, in relation to design and construction specifics and to drop conditions. Froude number scaling, on the other hand, becomes more obvious when considering the so-called load factor $F_{\max}/W$ [4,12,20,21]. In this context, using Eqs. (12) and (13) together with the definition of the Froude number $F_r \equiv V_{\text{ls}}^2/gD_0$ yields these results:

Horizontal inflation

$$\frac{F_{\max}}{W} = F_r \frac{D_0}{\sqrt{(SC_D)_{\text{sd}}}}\left[\frac{1}{n_{\text{fill}}^{\text{gen}}}\right] = F_r\left[\frac{1}{n_{\text{fill}} I_F^{\text{if}}}\right] \qquad V_i \gg V_f \tag{14}$$

Vertical inflation

$$\frac{F_{\max}}{W} = F_r \frac{D_0}{\sqrt{(SC_D)_{\text{sd}}}}\left[\frac{1}{n_{\text{fill}}^{\text{gen}}}\right]\left(1 + \frac{n_{\text{fill}}}{F_r}\right) = F_r\left[\frac{1}{n_{\text{fill}} I_F^{\text{if}}}\right]\left(1 + \frac{n_{\text{fill}}}{F_r}\right) \qquad V_i \gg V_f \tag{15}$$

It is interesting to note that the Froude factor appearing in the numerator of both Eqs. (14) and (15) follows from the particular V^2 dependence of aerodynamic drag, not from considering the ratio of initial kinetic energy relative to gravitational energy. This is particularly clear in the case of horizontal trajectories, in which gravity contributes no impulse or energy and yet displays a

dependence on F_r. Genuine Froude number dependence appears through the gravitational impulse n_{fill}/F_r term in Eq. (15), an expected result given that the equation deals with vertical trajectories. In this context, it is interesting to note that parachutes inflating along a horizontal trajectory open softer than the same parachutes inflating along vertical trajectories, at the same values of payload weight, filling time, altitude, and initial speed. This, of course, results from gravity supplying extra momentum to the system when deployed vertically.

These two equations also make clear what is left out when plotting the product $n_{\text{fill}}F_{\max}/W$ vs F_r for all parachute data (including for any trajectory types), as Niemi [25] did in his analysis of C-9 canopy data: here, only data collected along horizontal trajectories will display a near one-to-one relationship with F_r. On the other hand, the data connected with nonhorizontal trajectories will show a scatter that is driven mainly by the n_{fill}/F_r term, a scatter that reflects differences in design features as well as filling time and initial speed variations on a drop-to-drop basis.

Low Mass-Ratio Regime

Intuitively, the C_k data collected from inflation events taking place in wind or water tunnels should represent the zero mass-ratio limit of the opening shock factor, a limit that would also involve the MGI integral converging to a zero value. Given that $\Gamma \to 0$ as $R_m \to 0$ for both horizontal and vertical trajectories, there is a good chance that the ratio Γ/R_m will converge to the same value for any trajectory (i.e., vertical, horizontal, or two-dimensional) as $R_m \to 0$. On the other hand, n_{fill} will converge as $\sim R_m +$ constant in the limit $R_m \to 0$, as past studies have suggested [20,26,28]. Thus, to the extent that the drag integral also converges to a narrow range of values (as suggested in the previous section), the opening shock factor corresponding to low mass-ratio cases could be derived as follows, after using Eqs. (6–8) and (11):

$$\begin{aligned} C_k|_{\text{tunnel}} &\equiv \lim_{R_m \to 0;\, \Gamma \to 0} C_k \\ &= \frac{1}{n_{\text{fill}}} \frac{\sqrt{(SC_D)_{\text{sd}}}}{D_0} \left[\lim_{R_m \to 0;\, \Gamma \to 0} \left(\frac{2\Gamma}{R_m I_F^{\text{if}}} \right) \right] \\ &\equiv U_{\text{ck}} \frac{1}{n_{\text{fill}}} \frac{\sqrt{(SC_D)_{\text{sd}}}}{D_0} \end{aligned} \tag{16}$$

Here, n_{fill} would correspond to the zero mass-ratio limit of the filling time, and U_{ck} would be a nondimensional constant. The latter can be estimated by using Eq. (16) in conjunction with the tunnel data of [1,13,14] (including their C_k values). The results are as follows: $U_{\text{ck}} \sim 23$ for cruciform parachutes [1], $U_{\text{ck}} \sim 17$ for flat circular parachutes (full scale [1]), $U_{\text{ck}} \sim 15$ for flat circular parachutes (subscale [14]), $U_{\text{ck}} \sim 22$ for ribbon parachutes [1], and $U_{\text{ck}} = 22 \pm 4$ for disk-gap-band parachutes [13] (with the "squidding" phase excluded). Note that all of these parachutes were unreefed. Note also that the filling times and C_k data of [1] may not have been collected during the same tunnel run and most likely correspond to the inflation performance of different parachutes of the same type. Finally, the U_{ck} value measured on the subscale models of [14] is characterized by a value of the Reynolds number that is significantly lower than that of full-scale parachutes. But having U_{ck} being pretty much in the same range for all these different porosities and tunnel speeds should be tantalizing enough to warrant further investigation. In particular, more studies are needed to get U_{ck} values of parafoils, of hemispherical parachutes that are permanently reefed or disreefing, and of parachutes falling along nonhorizontal trajectories.

In the event of a little-changing U_{ck}, a simple formula for $F_{\max}$ can be derived from Eqs. (1), (6), and (16) as follows, being applicable to horizontal, vertical, or any two-dimensional fall trajectories:

$$F_{\max} = (SC_D)_{\text{sd}} \left(\frac{1}{2} \rho V_{\text{ls}}^2 \right) \left[\frac{U_{\text{ck}}}{n_{\text{fill}}} \frac{\sqrt{(SC_d)_{\text{sd}}}}{D_0} \right] \qquad U_{\text{ck}} \sim 15\text{–}22 \tag{17}$$

unreefed

As with Eqs. (12) and (13), Eq. (17) can be used to compute the load factor in order to further clarify Froude number scaling:

$$\frac{F_{\max}}{W} = \frac{1}{2} F_r \left[\frac{U_{\text{ck}} R_m}{n_{\text{fill}}} \right] \qquad R_m \ll 1 \tag{18}$$

Note that the load factor converges to

$$F_{\max}/W \propto R_m F_r / n_{\text{fill}}^{\text{gen,acft}} \to 0$$

in this range of mass ratio, an expected result. Note also that comparing Eqs. (12) and (13) with Eq. (18) shows that $F_{\max}/W$ is proportional to F_r in both large- and low-R_m limits, but with different proportionality factors.

Interestingly, Eq. (17) may explain some well-known facts about the differing $C_k|_{\text{tunnel}}$ values corresponding to the same parachute design but built at different sizes and for different applications. In the case of the ringslot parachute, for example, investigators have found $C_k|_{\text{tunnel}} \sim 1.0$ for the descent version used to stabilize payload during free-fall [1] and $C_k|_{\text{tunnel}} \sim 1.4$ for the pilot chute version used to extract other parachutes out of their container at very high speeds [1]. Equation (17) provides the correct opening shock factor estimate, considering that the former is characterized by $n_{\text{fill}} = 14$ [1] vs $n_{\text{fill}} = 5$–10 for the latter. Compared with their descent brethren, pilot chutes are not only smaller but also stored and folded in containers that are typically larger in size relative to their construction diameter. Moreover, very small parachutes tend to be a lot stiffer at the skirt. Such a design feature will generate larger initial canopy mouth areas (relative to actual constructed diameter) and, with the help of their associated lower porosities, lead to shorter filling times.

More Parachute Inflation Facts

Although very simple, Eqs. (12), (13), and (17) are approximations that point to several general and interesting truths about $F_{\max}$, in either the low or high mass-ratio regimes:

1) The swifter, the harder the opening: $F_{\max}$ being inversely proportional to the duration of the inflation process follows from the simple fact that the momentum transfer (per unit mass and per unit initial speed) during inflation is roughly the same for all parachutes, at least at high R_m, because of being deployed at similar speeds (as determined by aircraft or by payload free-fall characteristics) and descending steadily at the similar rates (as determined by landing speed requirements).

2) Strong vs weak dependence on mass ratio: The value of $F_{\max}$ corresponding to a given parachute design (porosity and reefing) and construction dimensions may or may not change significantly when R_m is changed, by either tuning payload mass or deployment altitude. The result depends on whether the system is characterized by a large- or small-R_m value before the change. For example, two identical parachutes characterized by the same $1/2\rho V_i^2$ and n_{fill} but with different payload weights will inflate with different $F_{\max}$, with the higher force being experienced by the system attached to the higher payload if R_m has values in the medium-to-high range for both weights. On the other hand, the change in $F_{\max}$ will be minimal if the two weights put the system in the low-R_m range. Of course, changing suspended weights from a very low R_m to a very high R_m (or vice versa) will lead to the largest changes in maximum drag sustained. All of this can be seen in Fig. 2, which shows C_k rising steeply in the medium-to-high range of mass ratios, while showing little variation in the low R_m limit of the graph.

3) Altitude dependence of opening shock: Another mass-ratio effect is the dependence of $F_{\max}$ on deployment altitude, which will be discussed Here, while assuming the same values of payload weight, canopy constructions, n_{fill} value, and initial value of $1/2\rho V_i^2$. (The latter should remain nearly the same at any altitude if the drops are launched from aircraft flown at the same indicated speed.) Again $F_{\max}$ is much more sensitive to the change if the system is characterized by a medium-to-high R_m (at both altitudes) than if characterized by a low R_m (again at both altitudes). For example, changing deployment altitudes from 2000 to 20,000 ft, as is

frequently done in many military applications, is accompanied by a 100% change in atmospheric density and inverse mass ratio. According to Eq. (12) (i.e., the high R_m result), a change in atmospheric density will result in the maximum force changing in a proportion given by

$$(F_{\max}^{\text{high alt}}/F_{\max}^{\text{low alt}}) \sim (\rho^{\text{low alt}}/\rho^{\text{high alt}})^1$$

indicating a significant increase in maximum force at the higher altitudes. According to Eq. (17), on the other hand (i.e., the low-R_m result), the change in force goes as

$$(F_{\max}^{\text{high alt}}/F_{\max}^{\text{low alt}}) \sim (\rho^{\text{low alt}}/\rho^{\text{high alt}})^0$$

that is, very little change. This confirms what has been empirically known for a long time [1], namely, that personnel parachute systems are much more sensitive to changes in deployment altitude than are drogues and aircraft deceleration chutes. (Again, note that this discussion rests on assuming small R_m dependence for n_{fill}, an assumption that should remain valid at deployment altitudes less than 100,000 feet [27].)

4) Dependence on canopy porosity and/or reefing: As documented in more detail in Knacke [1], canopy porosity and permanent skirt reefing (on hemispherical canopies) translate into different values of the steady-state descent drag area $(SC_D)_{\text{sd}}$, which in turns results in different values of the mass ratio. But these two design features translate into differing n_{fill} as well, typically to higher values for reefed or unreefed porous canopies, and also to larger n_{fill}, values for imporous or porous canopies with skirt reefing (as compared with imporous canopies with no reefing [1]). Typically, skirt-reefed canopies have longer filling times, because their mouth is constrained to smaller radii by the reefing line during the entire inflation sequence, thereby reducing the rate of the air mass entering the canopy. Porous canopies feature their longer filling time because of the internal pressure buildup rate being reduced by the constant exit of air through the vents and slots that are cut in them. According to Eqs. (12), (13), and (17), porosity and skirt-reefing considerations will result in changes in $F_{\max}$ in a proportion that is set mostly by the ratios $(SC_D)_{\text{sd}}/(R_m n_{\text{fill}})$ and $(SC_D)_{\text{sd}}^{3/2}/(n_{\text{fill}})$, respectively.

5) Inflation with permanent reefing vs no reefing: Comparing two identical systems inflating at the same $1/2\rho V_i^2$, but with one outfitted with (permanent) skirt reefing and the other with no reefing, the ratio of maximum forces sustained would be as follows, for horizontal trajectories and at high R_m [Eq. (12)]:

$$\begin{aligned}(F_{\max}^{\text{perm reefing}}/F_{\max}^{\text{no reefing}}) &\sim [(SC_D)_{\text{sd}}/(R_m n_{\text{fill}})]_{\text{perm reefing}} \\ &\times [(R_m n_{\text{fill}})/(SC_D)_{\text{sd}}]_{\text{no reefing}} \\ &\sim [(SC_D)^{1/2} n_{\text{fill}})]_{\text{no reefing}}/[(SC_D)^{1/2} n_{\text{fill}})]_{\text{perm reefing}}\end{aligned}$$

Given that

$$[(SC_D)_{\text{sd}}]_{\text{perm reefing}} < [(SC_D)_{\text{sd}}]_{\text{no reefing}}$$

[1,2] and that

$$(n_{\text{fill}})_{\text{perm reefing}} > (n_{\text{fill}})_{\text{no reefing}}$$

the force ratio could go either way, that is, being larger or smaller than unity, depending on the specific values of the drag areas and filling times. Thus the use of permanent reefing as an opening shock control device may not always work that way when used with a large-R_m system. At low R_m, on the other hand, Eq. (17) yields

$$\begin{aligned}(F_{\max}^{\text{perm reefing}}/F_{\max}^{\text{no reefing}}) &\sim [(SC_D)_{\text{sd}}^{3/2}/(n_{\text{fill}})]_{\text{perm reefing}} \\ &\times [(n_{\text{fill}})/(SC_D)_{\text{sd}}^{3/2}]_{\text{no reefing}}\end{aligned}$$

a result that unambiguously supports the benefit of (permanent) reefing for lowering $F_{\max}$ in this range of mass ratios; a fact that is strongly supported by empirical data. (Note: the proportion calculated here assumes a nearly constant U_{ck}, or at least one that has smaller values for reefed parachutes.)

6) Inflation without reefing vs with disreefing: Here, a comparison is made between two identical parachute–payload systems inflating at the same $1/2\rho V_i^2$ again, but with one system featuring no reefing and the other outfitted with disreefing, that is, with either a slider [11,24] or a skirt-reefing line being severed by a line cutter during inflation [1,2]. In this case one assumes the same values of $(SC_D)_{\text{sd}}$ and R_m, thus leaving the filling time as the main design factor reflecting the design change. In the light of the previous discussion (i.e., item 4), the maximum force sustained would compare as follows, again for horizontal trajectories at high R_m [using Eq. (12)]:

$$\begin{aligned}(F_{\max}^{\text{with reefing}}/F_{\max}^{\text{no reefing}}) &\sim [(SC_D)_{\text{sd}}/(R_m n_{\text{fill}})]_{\text{with reefing}} \\ &\times [(R_m n_{\text{fill}})/(SC_D)_{\text{sd}}]_{\text{no reefing}} \sim (n_{\text{fill}})_{\text{no reefing}}/(n_{\text{fill}})_{\text{with reefing}}\end{aligned}$$

Typically, slider disreefing increases the filling time compared with the unreefed configuration, thus leading to a reduction of the maximum force sustained in the inverse proportion of the filling time. With skirtline disreefing used in the large R_m regime, on the other hand, the situation is not so clear, because disreefing may increase or decrease the filling time depending on the timing of cutter activation.

Conclusions

This paper has shown that plotting C_k vs R_m has great potential for parachute design once the notion of filling time has been properly introduced via the use of the momentum-impulse theorem. The method also provides a theoretical framework that allows clearer thinking on the scaling of parachute inflation data with respect to selected design features and/or drop conditions. But it must be stressed that the approach will yield $F_{\max}$ estimates with potentially large uncertainties, uncertainties that have nothing to do with lack of knowledge or measurement errors. Rather, these have to do with the inherent scatter of the data in Figs. 2 and 3, caused by Γ and n_{fill} being defined over a range of values (in each figure) and with n_{fill} changing on a drop-to-drop basis. In other words, the method will provide a range of expected $F_{\max}$ values that would result over repeated uses of the designed parachute system, during which different initial trajectory flight angles and parachute mouth states may be sustained.

As for future work, the method would benefit greatly from further collection of C_k, Γ, and n_{fill}, data, not only to fill the gaps in Figs. 2 and 3, but also to yield altogether new C_k–R_m graphs characterized by smaller ranges in $n_{\text{fill}}^{\text{gen}}$. Moreover, the extra Γ data would help in determining to what extent variations of the MGI integral are the same for all parachute design types. These compilations would also help greatly in establishing the set of U_{ck} values to be used in Eqs. (16) and (17).

Acknowledgments

This work was performed with funding from the Natick Soldier Center (Natick, MA) under U.S. Army contract no. W9124R06P1068. The author wishes to thank the following individuals for the many fruitful discussions he has enjoyed: R. Charles, K. Desabrais, C. K. Lee, and J. A. Miletti from Natick Soldier Center; and G. Peek from Industrologic, Inc. Many thanks also to D. Wolf, K. Desabrais, and H. Johari for sharing their inflation drag data. Similar appreciation goes to J. Cruz (NASA Langley Research Center), NASA Ames Research Center, and Pioneer Aerospace for making available the tunnel drag data discussed in [13].

References

[1] Knacke, T. W., *Parachute Recovery Systems Design Manual*, Para Publishing, Santa Barbara, CA, 1992.

[2] Ewing, E. G., Bixby, H. W., and Knacke, T. W., "Recovery Systems Design Guide," U.S. Air Force Flight Dynamics Laboratory, Rept. AFFL-TR-78-151, Wright–Patterson AFB, Dec. 1978, pp. 254–257.

[3] Wolf, D., "Opening Shock," AIAA Paper 99-1702, 1999.

[4] Lee, C. K., "Modeling of Parachute Opening: an Experimental Investigation," *Journal of Aircraft*, Vol. 26, No. 5, 1989, pp. 444–451.

[5] Berndt, R. J., and DeWeese, J. H., "A Filling Time Prediction Approach for Solid Cloth Type Parachute Canopies," *2nd AIAA Aerodynamic Decelerator Systems Technology Conference*, AIAA, New York, 1966, pp. 17–32.

[6] Lingard, S. J., "Ram-Air Parachute Design," *AIAA Aerodynamic Decelerator Systems Technology Seminar*, AIAA, New York, 1995, p. 63.

[7] Potvin, J., Peek, G., Brocato, B., Kutz, R., Manglano, C., and Yavitz, B., "Deceleration Dynamics of Unreefed Cruciform and Flat Circular Parachutes During and After Inflation," *16th AIAA Aerodynamic Decelerator Systems Technology Conference and Seminar*, AIAA, Reston, VA, 2001, pp. 224–234; also, AIAA, Paper 2001-2028.

[8] Heinrich, H. G., and Hektner, T. R., "Flexibility as a Model Parachute Performance Parameter," *Journal of Aircraft*, Vol. 8, No. 9, 1971, pp. 704–709.

[9] Lee, C. K., and Sadeck, J. E., "Controlled Opening Method for Clustered Parachutes," *Journal of Aircraft*, Vol. 29, No. 2, 1992, pp. 264–272.

[10] Potvin, J., and Peek, G. E., "Inflation and Steady-Descent Characteristics of Truncated Cone Decelerators," *18th AIAA Aerodynamic Decelerator Systems Conference and Seminar*, AIAA, Reston, VA, 2005; also AIAA Paper 2005-1620.

[11] Butler, M., and Crowe, M., "Design, Development and Testing of Parachutes Using the BAT Sombrero Slider," AIAA Paper 99-1708, 1999.

[12] Doherr, K.-F., "Extended Parachute Opening Shock Estimation Method," AIAA, Paper 2003-2173, 2003.

[13] Cruz, J. R., Kandis, M., and Witkowski, A., "Opening Loads Analyses for Various Disk-Gap-Band Parachutes," AIAA Paper 2003-2131, 2003.

[14] Johari, H., and Desabrais, K. J., "Stiffness Scaling for Solid-Cloth Parachutes," *Journal of Aircraft*, Vol. 40, No. 4, 2003, pp. 631–638.

[15] Wolf, D., "A Simplified Dynamic Model of Parachute Inflation," *Journal of Aircraft*, Vol. 11, No. 1, 1974, pp. 28–33.

[16] Macha, J. M., "A Simple Approximate Model of Parachute Inflation," AIAA Paper 93-1206, 1993.

[17] Cuthbert, P. A., and Desabrais, K. J., "Validation of a Cargo Airdrop Software Simulator," AIAA Paper 2003-2133, 2003.

[18] Potvin, J., and Peek, G., "Inflation Study of U.S. Army Parachutes," U. S. Army, Contract Rept. W9124R-04-P-1272, Yuma Proving Ground, AZ, 21 Apr. 2005.

[19] Zell, P. T., Cruz, J. R., and Witkowski, A., "Structural Testing of Parachutes in the National Full-Scale Aerodynamics Complex 80 by 120 foot Wind Tunnel at NASA Ames Research Center," AIAA Paper 2003-2130, 2003.

[20] Lingard, J. S., "A Semi-Empirical Theory to Predict the Load-Time History of an Inflating Parachute," AIAA, Paper 84-0814, 1984.

[21] Lee, C. K., "Experimental Investigation of Full-Scale and Model Parachute Opening," AIAA Paper 84-0820, 1984.

[22] Lee, C. K., Lanza, J., and Buckley, J. "Experimental Investigation of Clustered Parachute Inflation," AIAA Paper 97-1478, 1997.

[23] Potvin, J., Peek, G., and Brocato, B. "New Model of Decelerating Bluff Body Drag," *Journal of Aircraft*, Vol. 40, No. 2, 2003, pp. 370–377.

[24] Potvin, J., Peek, G., and Brocato, B., "Modeling the Inflation of Ram-Air Parachutes Reefed with Sliders," *Journal of Aircraft*, Vol. 38, No. 5, 2001, pp. 818–827.

[25] Niemi, E. E., Jr., "An Impulse Approach for Determining Parachute Opening Loads for Canopies of Varying Stiffness," AIAA Paper 91-0874, 1991.

[26] Fu, K-H., "Theoretische Untersuchung zum Füllungsvorgang Eines Flexiblen Fallschirm-Last-Systems (Theoretical Study of the Filling Process of a Flexible Parachute Payload System)," German Air and Space Research and Test Institute, Rept. DLR-FB 75-56, Braunschweig, Germany, 1975.

[27] Barnard, G. A., "The Effect of Extreme Altitude of Parachute Filling Distance," AIAA Paper 93-1207, 1993.

[28] Heinrich, H. G., "The Opening Time of Parachutes Under Infinite Mass Conditions," AIAA Paper 68-12, 1968.

[29] Heinrich, H. G., "The Opening Time of Parachutes Under Infinite Mass Conditions," *Journal of Aircraft*, Vol. 6, No. 3, 1969, pp. 268–272.

[30] Pflanz, E., "Zur Bestimmung der Verzoegerunskraefte bei Entfaltung von Lastenfallschirmen," *Forschungsanstalt Graf Zeppelin*, Vol. 231, Bericht, Stuttgart-Ruit, Germany, 1942; also ZWB FB 1706, 1942.

[31] Ludtke, W. P., "A Technique for the Calculation of the Opening-Shock Forces for Several Types of Solid Cloth Parachutes," *4th AIAA Aerodynamic Decelerator Systems Technology Conference*, AIAA, New York, 1973, pp. 176–185; also AIAA Paper 73-477.